Catalysis Letters
https://doi.org/10.1007/s10562-019-02813-8

Adsorption and Photodegradation of Acetaldehyde and Ethylene on TiO_2 (001) Surface: Experimental and First Principle Studies

Gansheng Shi[1] · Asad Mahmood[1] · Guanhong Lu[1] · Xiao Wang[1] · Shengrui Tong[2] · Maofa Ge[2] · Xiaofeng Xie[1] · Jing Sun[1]

Received: 25 January 2019 / Accepted: 7 May 2019

Abstract

In this work, the adsorption and photodegradation of acetaldehyde and ethylene on TiO_2 nanoparticles (NPs) with dominant {001} facets were studied. Additionally, the first principle calculation was used to complement the experimental results. TiO_2 NPs were synthesized by using a hydrothermal method. The experimental results indicated that adsorption amount of acetaldehyde on TiO_2 {001} facets is higher than ethylene, with the initial concentration as 500 ± 10 ppm. Photodegradation efficiency of 88% was achieved for acetaldehyde in contrast to 17% for ethylene at flow rate of 10 sccm. The first principle calculations show that the adsorption energy (E_{ads}) for acetaldehyde is 0.603 eV and that of ethylene is 0.251 eV. This study is imperative for understanding the adsorption and photodegradation process of acetaldehyde and ethylene, two typical VOCs, and helpful to design the photocatalysts with high efficiency.

Graphical Abstract

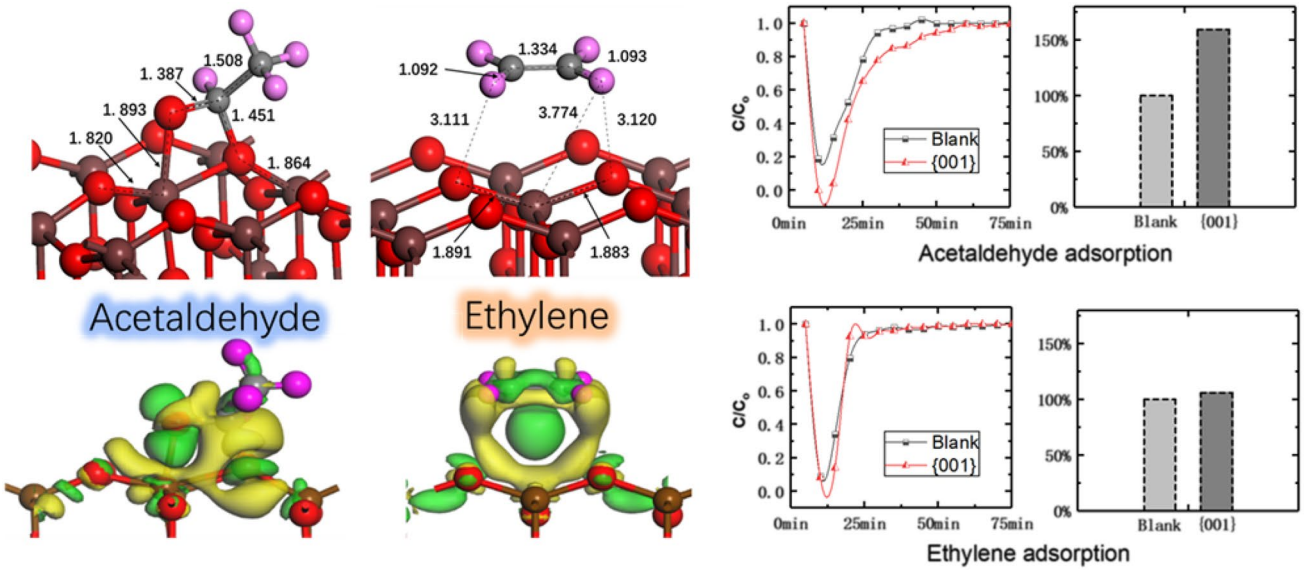

Keywords Ethylene · Acetaldehyde · TiO_2 (001) surface · Saddle-like structure · Carbonyl group · Adsorption mechanism

1 Introduction

Volatile organic compounds (VOCs) are produced in the environment by natural and anthropogenic activities that can cause serious health problems [1, 2]. Regardless of its

✉ Jing Sun
jingsun@mail.sic.ac.cn

Extended author information available on the last page of the article

Published online: 20 May 2019

hazardous effect, VOCs additionally participate in different reactions in the atmospheric environment, for instance, reacting with ozone (O_3) and NOx to form secondary organic aerosols and further causing particulate matter pollution ($PM_{2.5}$ and PM_{10}). To this end, strategies have been adopted to address this issue, such as removal through adsorption and destruction that involves VOCs degradation by different oxidation process [3]. However, a single approach is not sufficient, thus, a consolidated methodology containing more than one procedure is used. The photocatalytic oxidation (PCO) of VOCs is a promising method for air purification of which photocatalysts for example, TiO_2 [2], ZnO [4], WO_3/Bi_2WO_6 [5], and γ-Al_2O_3 [6] have been widely used. Among these, TiO_2 is a stable, nontoxic, and low cost photocatalysts, which has been broadly considered for numerous electrical and photocatalytic applications, for example, photoelectrochemical water splitting [7], photodegradation of hazardous components in water and air [8, 9], phenol oxidation [10], and supercapacitors [11].

Ethylene and acetaldehyde are delivered in the air through natural and industrial sources. Even a small concentration [parts-per-million (ppm) to parts-per-billion (ppb)] of ethylene is physiologically exceptionally active that acts as an aging (ripening) agent and cause substantial deterioration of fresh fruits and vegetables during shipping and storage [12]. A small concentration of ethylene can cause 10% to 80% of the product loss amid these operations. It has been reported that $(18-45)\times10^6$ tons of ethylene is annually released by natural (74%) and anthropogenic sources (26%) [13, 14]. Thus, it is imperative to remove ethylene in storage and handling environment. The PCO of ethylene has been reported to follow the Langmuir–Hinshelwood type of kinetic, which is converted into CO_2 according to the reaction: $C_2H_4 + 3O_2 \rightarrow 2CO_2 + 2H_2O$ in the presence of TiO_2 and UV light [15–17]. However, the underline mechanism of ethylene adsorption and PCO is yet vague. For instance, different endeavors have been accounted for to research PCO of ethylene, yet, no mechanism could have been developed because most of the studies detected only ethylene in the photoreactor outlet. The PCO efficiency of ethylene has been found to increase with increasing ethylene concentration between 53 and 346 ppm, which can be associated with gas supply [18]. Likewise, Park et al. [19] reported the conversion of ethylene into CO_2, CO, and H_2O at room temperature. Ethylene is first oxidized to CO through $C_2H_4O^*$ radical formation, which further oxidizes into CO_2 through reaction: $O^* + C_2H_4 \rightarrow \left(C_2H_4O\right)^* \rightarrow CO \rightarrow CO_2$. They recommended that reactive hydroxyl ($OH^\bullet$) and oxygen species ($O_2^{\bullet-}$, $O_3^{\bullet-}$) on catalyst surface play an essential role in PCO of ethylene. As opposed to this mechanism, Yamazaki et al. [18] reported that ethylene reacts with OH radicals on the TiO_2 surface to form $C_2H_4OH^\bullet$ intermediates, which further reacts with oxygen species to form CO_2. In this regard, attempts have been reported to interpret the mechanism of ethylene adsorption and PCO. Acetaldehyde is another major indoor pollutant gas that belongs to carbonyl containing compounds group [20]. Due to industrialization and urbanization, the carbonyl-containing compounds are constantly increasing in the environment. They also participate in the formation of secondary aerosol and photochemical smog. Furthermore, the low molecular weight carbonyl containing compounds such as acetaldehyde and formaldehyde are mutagenic and carcinogenic by respiratory intake. Recent studies have shown the potency of commercially available nanosized and microsized TiO_2 powders for the photodegradation of common indoor air pollutants including toluene, acetone, and acetaldehyde [21]. Other attempts incorporate surface modification of TiO_2 by depositing metals (Ag, Pt, Au) NPs. It has been reported that formaldehyde can be completely oxidized to CO_2 and H_2O using 1% Pt/TiO_2 system at room temperature. The study confirmed that charge on Pt, dispersion of Pt NPs on TiO_2 surface, and surface oxygen species influence the photocatalytic activity. For example, negatively charged metallic Pt NPs and chemically adsorbed oxygen species on the surface exhibit superior photocatalytic activity [22].

For the gas phase PCO, the adsorption of gas molecules is inevitable the first step. As described in previous study [23], the rGO-TiO_2 hybrids significantly enhanced the degradation of gaseous VOCs by improving the adsorption ability compared to pure TiO_2. However, the adsorption mechanism of VOCs on TiO_2 is not clearly investigated. Before modifying the catalyst to improve the adsorption ability, the basic interaction between the gas molecules and pure catalyst surface should be figured out. In this way, it is very important to comprehend different surface features of a photocatalyst and the chemical structure of pollutant gas molecules to understand the adsorption mechanism. In addition, it has been reported that different facets of a similar semiconductor material display dissimilar electronic and optical properties due to variations in atomic arrangement and coordination on the surface [24, 25]. Under normal growth conditions, the anatase phase grows in tetragonal bipyramid shaped NPs with a high percentage of {101} facets and low {001} percentage. The coordination of titanium (Ti) atom on the surface plays a key role in the surface catalyzed reactions. For example, the (001) surface exhibit 50% of five-coordinated Ti (Ti_{5c}) atoms, while the (101) surface exhibit 100% of Ti_{5c} atoms. Thus, the {001} facets are considered more reactive for the surface catalyzed reactions. Along these lines, this study presents an in-depth analysis of adsorption and PCO oxidation of acetaldehyde and ethylene on TiO_2 {001} facets. It also provides comprehensive insight into the interaction energy of the two types of VOCs with TiO_2 {001} facets through DFT method, which offers a guideline to rationally design a photocatalyst for practical applications. Firstly, the

adsorption mechanism of acetaldehyde and ethylene was examined using dynamic adsorption tests and temperature programmed desorption (TPD). Next, the photocatalytic degradation experiment was performed under UV/visible irradiation. Also, the first principle calculation was used to study the adsorption mechanism on the molecular level. Various adsorption configurations were considered on TiO_2 (001) surface and their adsorption energies were calculated. Moreover, the highly stable adsorption complexes were further used to calculate the local density of states (LDOS) and electron density difference (EDD) to study the interaction of these gases on TiO_2 (001) surface.

2 Experimental

2.1 Chemicals

The chemicals and solvents used in this experiment are commercially available and were used without further purifications. The reagents used in this experiment are titanium butoxide ($C_{16}H_{36}O_4Ti$; 97%) and aqueous solution of hydrogen fluoride (HF: 40 wt%) from Sigma-Aldrich. Additionally, absolute ethanol (≥ 99.5%; Sigma-Aldrich) and deionized water were used as solvents. Deionized water with a resistivity of 18.2 MΩ cm was obtained through a Milli-Q Advantage A10 water purification system (Burlington, USA).

2.2 Synthesis of TiO_2 NPs with Dominant {001} Facets

The TiO_2 NPs were synthesized using strong acidic hydrothermal reaction using hydrogen fluoride (HF; 40 wt%). Initially, 70 mL of $C_{16}H_{36}O_4Ti$ was mixed with 4 mL of HF solution in a Teflon-lined reactor (100 mL). An aqueous solution of HF was used in this experiment. Then carefully closed the reactor and treated it at 200 °C for 24 h and subsequently cooled it down to room temperature. The as-prepared white powders were isolated using a high-speed centrifuge (10,000 rpm) and washed five times with deionized water (150 mL) and absolute ethanol (150 mL). The as-prepared product was dried overnight at 100 °C in an oven. Next, the powders were calcined at 550 °C for 2 h.

2.3 Characterization

The phase and morphology of TiO_2 NPs were studied using X-ray diffractometer (Model: Ultima IV 2036E102, Rigaku Corporation, Japan) with Gu Ka radiation ($\lambda = 0.15418$ nm, 2θ varied from 20° to 80°, 8°/min) using continuous method, the voltage is 40 kV and current is 40 mA. Transmission electron microscope spectra were collected on FEI Electron Optics microscope (Model: Tecnai G2 F20), respectively. A DXR Raman spectrometer (Thermal Scientific Corporation, USA) was used to study the Raman modes using a laser with an excitation wavelength of 532 nm at laser power of 7 mW. Photoluminescence (PL) spectrum was recorded by using Edinburgh FL/FS900 spectrophotometer with an excitation wavelength of 320 nm. TPD analyses were performed using a ChemiSorb PCA-1200 (Builer, China). Initially, 0.1 g of sample was taken in a quartz tube fixed inside an electric furnace to control the temperature. The sample was subjected to nitrogen flow to remove previously adsorbed surface species at 120 °C for 1 h. The sample was subsequently cooled down to room temperature. Next, the preselected gases ethylene (49.8 ppm) or acetaldehyde (50 ppm) were led to pass (flow rate of 30 mL/min^{-1}) the sample tube for 2 h to achieve the adsorption equilibrium. Finally, the high purity nitrogen was introduced, and the temperature was increased from room temperature up to 800 °C with a step size of 10 K/min^{-1}. In this way, desorption of sample gases was recorded in a broad temperature range. The photocatalytic degradation experiment was performed using continuous gas flow system coupled with gas chromatography. The detail of the experimental setup is given in previously published work [23]. 0.1 g of the sample was milled in absolute ethanol for 15 min and the slurry was deposited on the glass substrate (area = 60 cm^2) to develop films. The films were dried in an oven at 100 °C for 2 h. Next, the films were transferred to a closed chamber (20 × 10 × 1.5 cm) composed of inlet–outlet valves for gases and a xenon lamp at a distance of 30 cm. The adsorption and degradation of the gaseous pollutants were detected using gas chromatography.

2.4 Computational Detail

The first principle calculations were performed using Vienna Ab-Initio Simulation Package (VASP) [26–28]. The geometries of molecules in the gas and on TiO_2 (001) surface exhibiting different configuration were optimized using generalized gradient approximation (GGA) implemented by Perdew-Burke-Erzhenhof (PBE) [29, 30]. Initially, TiO_2 bulk was optimized using 2 × 2 × 2 supercell. The fully relaxed structure of bulk TiO_2 was cleaved along [001] direction in a 2 × 3 × 1 supercell containing 120 as total number of atoms. A vacuum of 20 Å was used for to avoid interaction of reflective mirror images. A cutoff energy of 400 eV was used in all calculations. The *k*-point grid was sampled as 2 × 3 × 1 in the Brillion zone. Also, to account for the weak Vander wall forces (vdW) between the gas molecules and TiO_2 (001) surface, vdW D correction method (DFT-D framework) given by Grimme was used [31]. The structure of the pure TiO_2 slabs were obtained using periodic boundary conditions with constraints on the coordinates of the bottom two layers. In the same condition, TiO_2 slabs with acetaldehyde or ethylene

bound on the surface were achieved. An ultrafast pseudopotential was used in all calculations. The adsorption energy (ΔE_{ads}) is calculated according to Eq. (1):

$$\Delta E_{ads} = \left(E_{Molecule} + E_{Surface}\right) - E_{Molecule/surface} \quad (1)$$

$E_{Molecule}$ is the energy of a molecule in the gas phase, $E_{Surface}$ is the slab energy without adsorption and $E_{Molecule/Surface}$ is the energy of the surface and molecule complex. The local and partial density of states (PDOS) were calculated for the most stable adsorption complex. Finally, the electron density difference was calculated to trace the electron rich and electron depleting regions.

3 Results and Discussion

Figure 1a shows the XRD pattern of TiO_2 NPs predominantly grown along the [001] direction. The XRD result suggested a well-crystalline single-phase anatase TiO_2. All of the diffraction peaks were indexed to standard JCPDS: 21-1272 [32]. Figure 1b–d shows the high-resolution transmission electron microscope (HRTEM) images for TiO_2 NPs. The surface morphology of the particles demonstrated well-dispersed square-shaped disk particles (Fig. 1c). However, a significant variation in the particle size was observed, suggesting a nonhomogeneous grain growth. Additionally, the lattice fringes were determined for the selected NPs and the average values were calculated as 0.35 and 0.237 nm (Fig. 1b). These values match well with the (101) and (004) anatase TiO_2 atomic planes, respectively. To further comprehend the microstructure and XRD data, selected area electron diffraction (SAED) (Fig. 1d) was carried out. It has been previously reported that the top surface of the anatase demonstrates the (001) facet and the lateral side demonstrate the (101) facet of TiO_2 NPs [33, 34]. The top surface SAED ring pattern fits well to the XRD data, where the diffraction rings were used to calculate the distance from the center. The corresponding high-resolution rings are associated with different atomic planes exhibiting high peak intensity in the diffraction pattern along (101), (004), (200), (211), (204), and (220). The XRD and HRTEM results confirmed well-crystalline single-phase TiO_2 NPs with dominant {001} facet. The specific surface area was calculated as 67 m^2/g.

The Raman spectroscopy was further performed to understand the structure of TiO_2 NPs (Fig. 2). All the Raman modes were matched with the previously reported results for the same type of anatase system [35]. The characteristic peaks for anatase TiO_2 were observed around 100 to 650 cm^{-1}. The peaks around 143 (symmetric stretching of Ti–O – Ti bonds), 195, and 396 cm^{-1} (symmetric bending vibrations) can be associated with $3E_g$, $2B_{1g}$, $1A_{1g}$ Raman modes [36]. The peak around 396 cm^{-1} is assigned to E_g modes. The peaks at 518 (antisymmetric bending vibrations) and 639 cm^{-1} are associated with the unresolved doublet and A_{1g}/B_{1g} and A_{1g}, respectively [37]. No other peaks can be observed, which further confirms the formation of single-phase anatase TiO_2 NPs. The inset figures show the UV–vis absorption and photoluminescence spectroscopy results for TiO_2 NPs. The fundamental absorption edge can be seen around 400 nm. Typically, the band gap of TiO_2 has been reported as 3.15 eV [38]. We calculated the band gap of TiO_2 as 3.2 eV, which is in good agreement with the previously reported values [39]. The observed difference in the

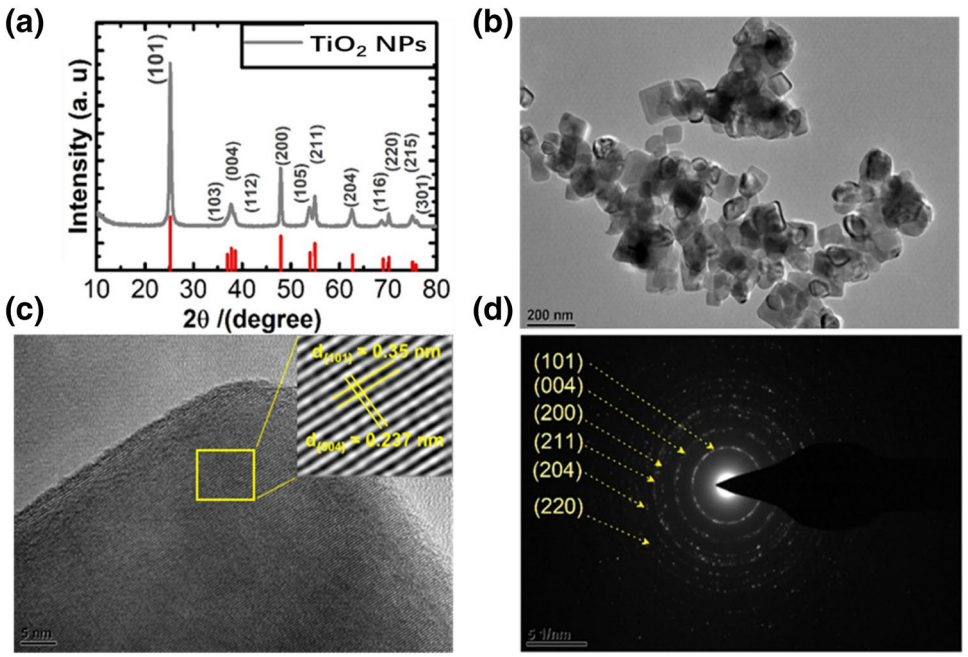

Fig. 1 **a** XRD pattern for the TiO_2 NPs, **b** HRTEM image of the lattice fringes of TiO_2, **c** TEM morphology of the TiO_2 nanoparticle, **d** diffraction ring pattern for the TiO_2

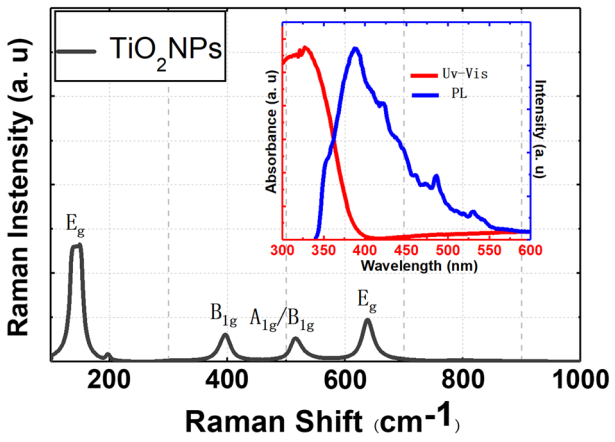

Fig. 2 Raman spectrum of the TiO_2 nanoparticles. The inset figure shows the UV–visible and photoluminescence spectrum of TiO_2 nanoparticles

band gap value can be associated with slight variations in crystal structure, which is responsible for variation of the optical band gap.

As stated earlier, for the photodegradation of gaseous reactions, it is pivotal that a gas molecule is adsorbed on the surface of TiO_2 that further reacts with reactive oxygen species such as oxide and hydroxyl radicles and subsequently decompose [23]. The absorption of light excites photoelectrons in the conduction band (CB) while holes are created in the valance band (VB). These electrons are responsible for the production of reactive oxygen species on the surface [40, 41]. Therefore, it is significant to understand the interaction of gaseous pollutants with a catalyst surface. Thus, the behavior of ethylene and acetaldehyde on TiO_2 {001} facets was experimentally studied. The adsorption and photocatalytic activity of TiO_2 NPs was studied using ethylene and acetaldehyde as model VOCs (1000 ± 10 ppm in gas cylinders) at a flow rate of 5 sccm. Air produced by an air generator was used as carrier gas which is adjusted at the same flow rate as the VOCs pollutants, in this way, the initial concentration of acetaldehyde and ethylene is fixed at 500 ± 10 ppm,and the corresponding flow rate was controlled at 10 sccm. Moreover, similar initial concentration (500 ± 10 ppm) of ethylene and acetaldehyde was used in this experiment at 10, 20, and 40 sccm, in which air accounts for half of the flowing gas. The adsorption efficiency (E) of the sample gases and the blank chamber was calculated using Eq. (2) and (3).

$$E_{catalyst} = \{[\int_0^t v \times (1 - C/C_0)\,dt]_{catalyst} / [\int_0^t v \times (1 - C/C_0)\,dt]_{blank}\} \times 100\,\% \quad (2)$$

$$E_{blank} = \{[\int_0^t v \times (1 - C/C_0)\,dt]_{blank} / [\int_0^t v \times (1 - C/C_0)\,dt]_{blank}\} \times 100\,\% = 100\% \quad (3)$$

where C_0 and C are initial gas concentration and at different time intervals, respectively, v is flow rate, t is the time interval of reaction. The results are given in Fig. 3. It can be seen that there is no significant increase in the adsorption ability of ethylene on the surface of TiO_2 contrasted to blank chamber. The results suggested only a 6% increase for ethylene adsorption compared to the blank chamber. In contrast to ethylene, the acetaldehyde demonstrated a higher adsorption efficiency (156%) under similar adsorption conditions. To further confirm these observations, the TPD experiment (Fig. 4) was conducted. This test can provide an insight into the interaction of the gaseous molecules on the surface of a photocatalyst. Both ethylene and acetaldehyde demonstrated peaks above 200 °C. The desorption peak of ethylene was observed at 318 °C, while the acetaldehyde exhibited a desorption peak around 485 °C. Based on these results, it can be inferred that the acetaldehyde molecules strongly bound on TiO_2 (001) surface in contrast to ethylene, thus a high temperature was required for the desorption of acetaldehyde from the catalysts surface.

To further study the adsorption behavior of ethylene and acetaldehyde, first principle calculations were performed. The geometrically optimized TiO_2 (001) surface is given in Fig. 5. The atomic configuration of TiO_2 (001) surface is different from (101) surface, which contains under coordinated five-fold Ti atoms (Ti_{5c}) [24, 42]. Similarly, two and three-fold oxygen atoms (O_{2c}, O_{3c}) are present at the surface. The under coordinated atoms are regarded as the active adsorption sites and render more reactivity to (001) surface contrasted to (101) surface. The angle between O_{2c}–Ti_{5c}–O_{2c} is calculated as 138.789°, while the bond distance between Ti_{5c} and O_{2c} is calculated as 1.8889 Å, which is closer to the previously reported values [43]. The fully relax structure was used for the ethylene and acetaldehyde adsorption exhibiting different configurations.

Figure 6 shows the adsorption of acetaldehyde and ethylene on TiO_2 (001) surface exhibiting different orientations (Ac_A to Ac_D). The corresponding adsorption energies are given in Table 1. The acetaldehyde molecule can attach to TiO_2 (001) surface through different bonds, for example, CH_3–, –C=O, and –H. Similarly, the carbonyl carbon atom (–C=O) can interact simultaneously with the Ti_{5c}–O_{2c} on the surface through C–O_{2c} and Ti_{5c}–Omol (Omol = O of the molecule). In the case of Ac–A configuration, the distance between the carbonyl O and Ti_{5c} is calculated as 2.394 Å, which is a larger value than the actual bond length between Ti_{5c}–O_{2c} of surface.

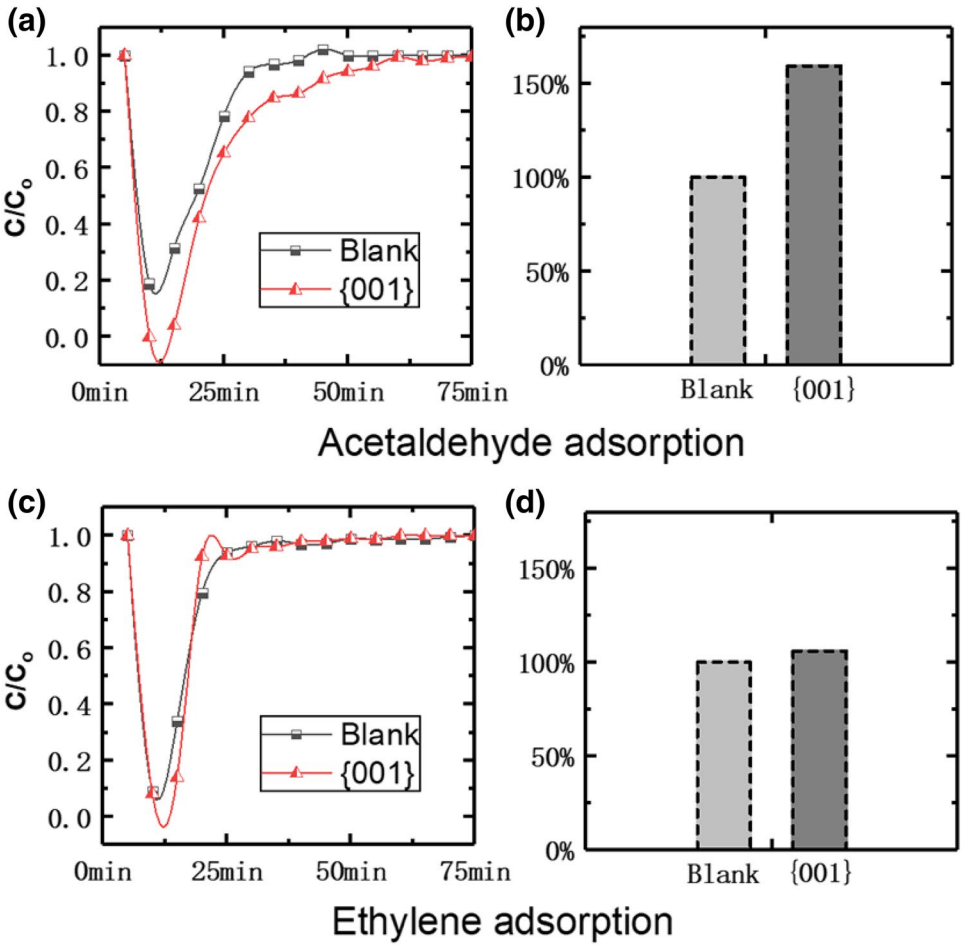

Fig. 3 Adsorption of VOCs in the absence and presence of TiO_2 nanoparticles; **a** adsorption of acetaldehyde, **b** adsorption efficiency of acetaldehyde, **c** adsorption of ethylene, **d** adsorption efficiency of ethylene

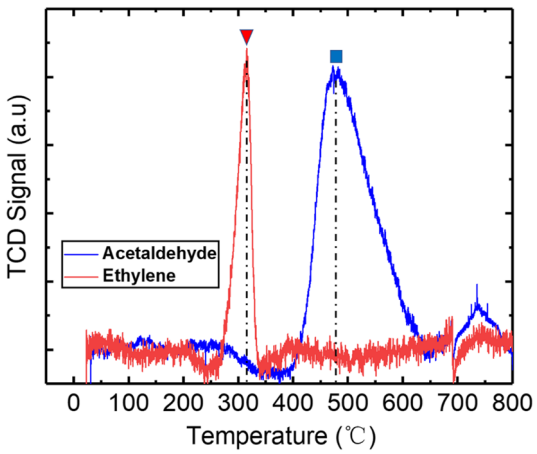

Fig. 4 Temperature programmed desorption of acetaldehyde and ethylene

Next, the distance between carbonyl H and O_{2c} is 2.438 Å. Moreover, no structural deformation can be seen on TiO_2 (001) surface. The corresponding adsorption energies for different acetaldehyde configuration on TiO_2 surface suggested low adsorption energies. Among these, the Ac_C exhibited a high adsorption energy value. In the case of Ac_C, the corresponding bond distance between carbonyl O of molecule and Ti_{5c} is calculated as 1.893 Å, which is almost similar to 1.889 Å (Ti_{5c}–O_{2c}). Similarly, the −C=O bond length (1.38 Å) was observed to increase for this adsorption mode in contrast to other configurations studied in this work. Also, the carbonyl C atom strongly interacted with the surface O_{2c} and almost pulled it out of the surface, suggesting the formation of a new chemical bond. Additionally, the surface of TiO_2 (001) demonstrated a significant distortion. The corresponding adsorption energy value for this structure has been calculated as 0.603 eV. These results suggest that acetaldehyde molecule interact with the surface through chemical bonds forming a saddle like structure, consequently, results in a strong interaction. In contrast to acetaldehyde, the adsorption energy values for ethylene are quite low. There is no significant bond formation or distortion on TiO_2 surface. Even when the initial position of the ethylene molecule was used as chemical interaction (not shown for the most part), the molecule moved away from the surface during simulation to minimize the energy of the adsorption complex to form a more stable geometry. The Et_B demonstrated higher

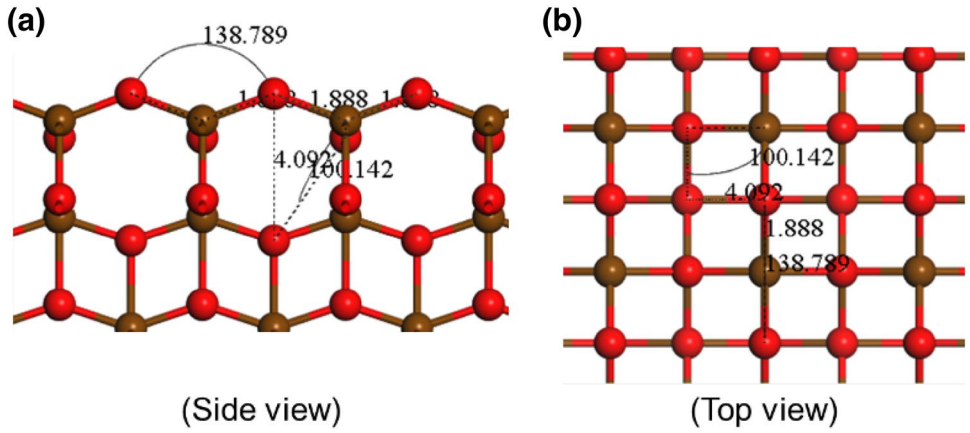

Fig. 5 Optimized structures of the **a** side view and **b** top view of anatase TiO_2 (001) surface. Ti and O atoms are labeled as dark brown and red spheres, respectively. The bond length is Å

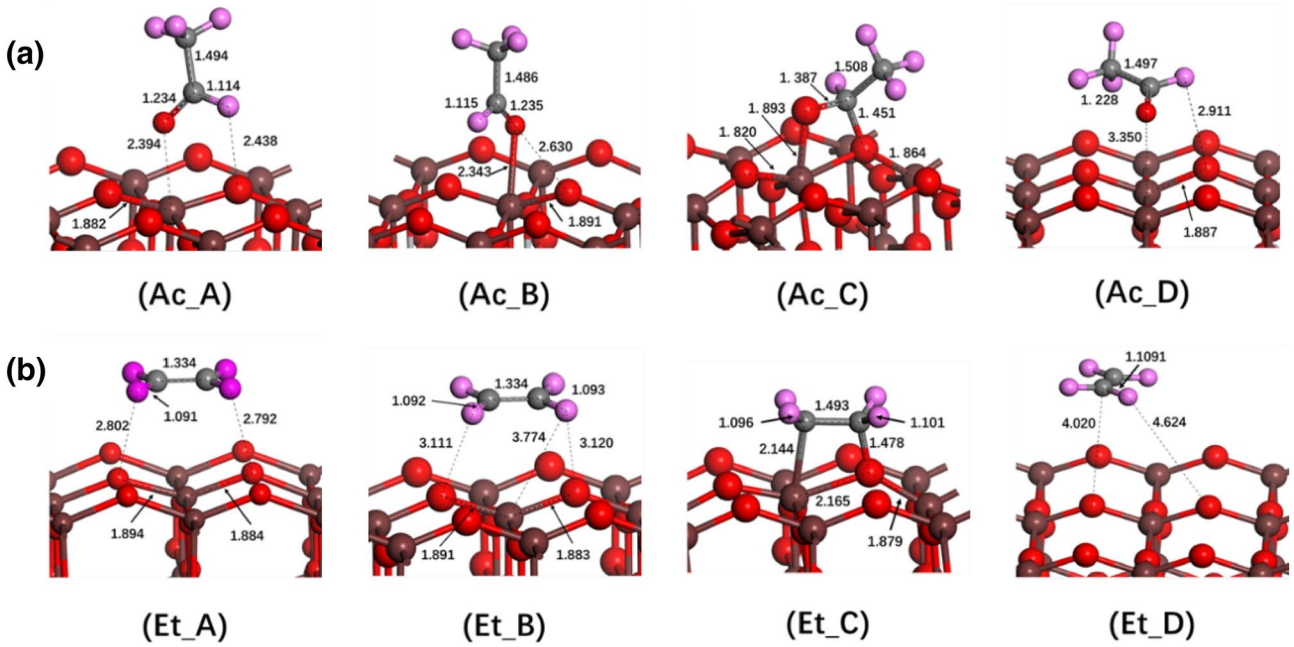

Fig. 6 Optimized geometries of selected VOCs on anatase TiO_2 (001) surface; **a** acetaldehyde, **b** ethylene. The carbon and hydrogen atoms are colored in dark gray and purple, while oxygen and titanium atoms are colored in red and dark brown, respectively. The number demonstrates the calculated bond length (unit: Å)

Table 1 Calculated adsorption energies of acetaldehyde and ethylene on TiO_2 (001) surface

Mode	E_{ads} (eV)	
	Ac	Et
A	0.35	0.101
B	0.115	0.251
C	0.603	−0.134
D	0.007	0.1867

adsorption energy (0.251 eV) compared to other ethylene configurations in this study. Therefore, it can be inferred that the carbonyl group in acetaldehyde play a significant role for adsorption on TiO_2 (001) surface. The LDOS and PDOS were further studied to understand the coupling between different atomic states. The corresponding LDOS for the surface, molecules, and different atoms are given in Fig. 7. The sharp peaks in Fig. 7a, j is the characteristic molecular peaks in the gas phase. The PDOS for the surface demonstrated that 3d-states of Ti strongly contributed in the lower CB exhibiting a comparatively small contribution in the upper VB (Fig. 7a, f). A small contribution can also be seen in the upper CB by Ti p-states. The oxygen 2p-states mainly contributed to the upper VB (Fig. 7b, g). The intensity of these peaks is significantly lower in contrast to acetaldehyde and ethylene in the gas phase suggesting more interaction. This behavior was further studied by

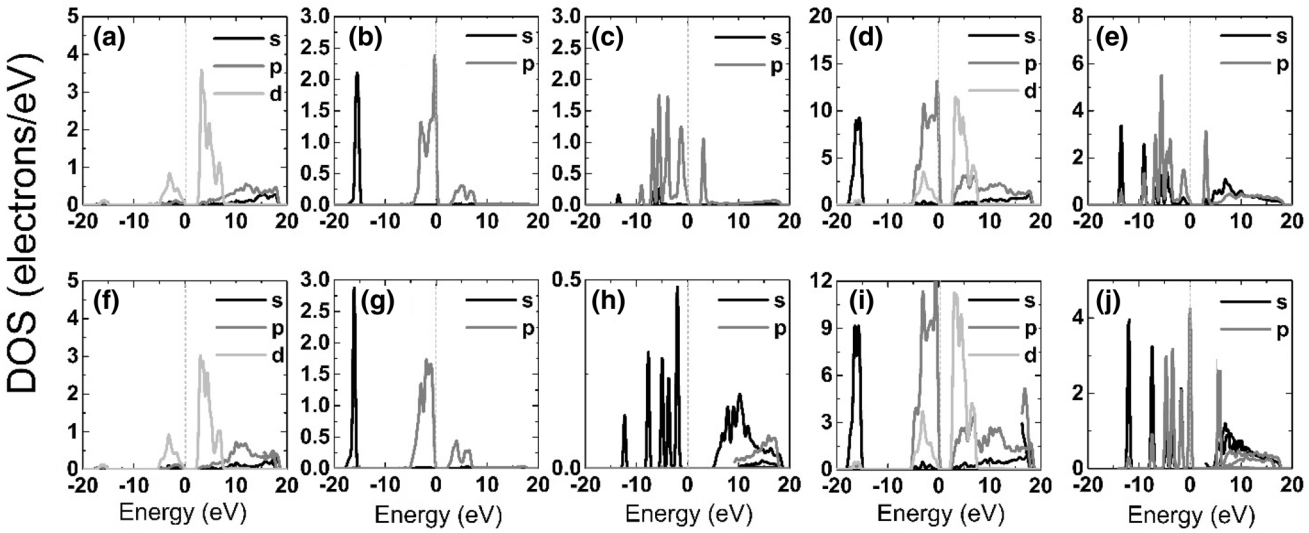

Fig. 7 Local density of states: **a**, **f** Ti_{5c}, **b**, **g** O_{2c}, **c** =O of acetaldehyde, **h** hydrogen of ethylene, **d**, **i** TiO_2 (001) surface before adsorption, **e**, **j** acetaldehyde and ethylene molecule in the gas phase. The Fermi energies are set as 0 eV

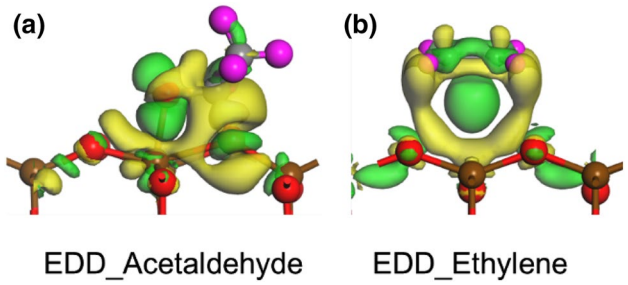

Fig. 8 Charge density difference for the acetaldehyde and ethylene adsorbed complex

the electron density difference. The more stable adsorption complex was used for calculating the EDD. The results are given in Fig. 8. The yellow color represents the electron depleting area while the green color shows the electron rich area. It can be seen that most of the electron rich area is surrounded by the carbonyl oxygen and surface O_{2c}. In contrast, the hydrogen atoms in ethylene do not show any significant interaction with the surface oxygen while the electron rich area is mostly around the double bond between the C=C of ethylene. These results further demonstrate the difference in behavior of ethylene and acetaldehyde molecules on TiO_2 (001) surface.

Finally, experiments were performed to compare the photocatalytic degradation of acetaldehyde and ethylene under different flow rate (Fig. 9). Initially, the gases were flown through the chamber in the dark and a saturated state was achieved in each experiment. Next, the 400 W xenon lamp was turned on for the photodegradation process. It can be seen that TiO_2 demonstrated a high photocatalytic degradation for acetaldehyde irrespective of the flow rate in contrast to ethylene. The photocatalytic activity was observed to

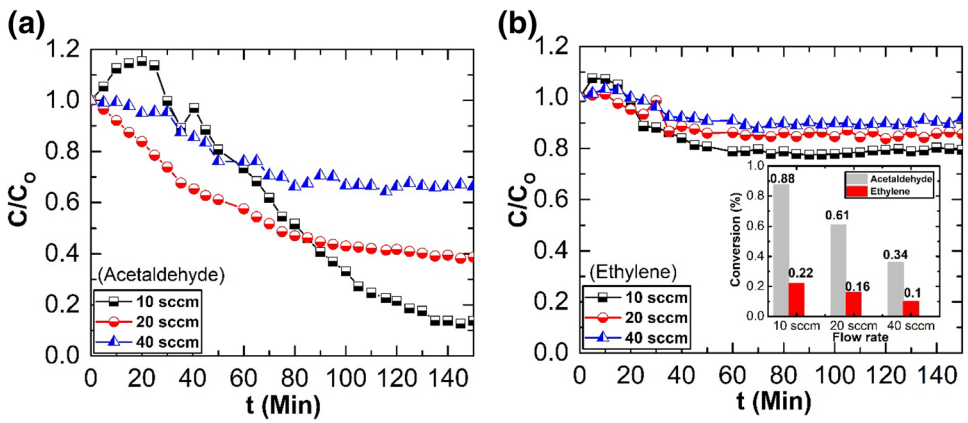

Fig. 9 Photodegradation of VOCs with different flow rate **a** acetaldehyde and **b** ethylene. The inset figure in **b** shows the degradation efficiency for acetaldehyde and ethylene at different flow rate

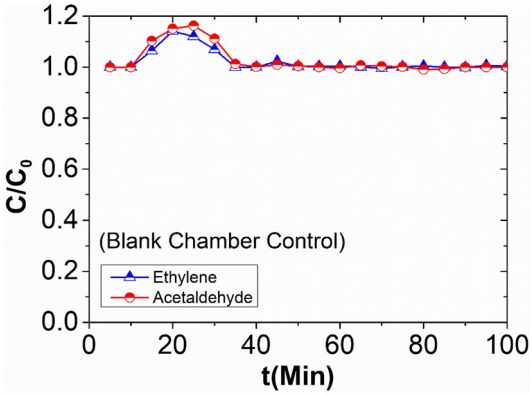

Fig. 10 Photodegradation of VOCs control experiment with flow rate of 10 sccm without TiO_2

decrease with increasing flow rate for both the gases studied in this work. Initially, when the flow rate was 10 sccm, 88% of acetaldehyde was degraded. By increasing the flow rate (20 and 40 sccm) the photodegradation efficiency significantly decreased to 61% and 34%, respectively. However, poor photodegradation behavior was observed in the case of ethylene. Moreover, the flow rate has not significantly affected the photodegradation efficiency, which further confirms the poor interaction of ethylene on TiO_2 {001} facets. This behavior can be associated with the fact that with increasing flow rate the retention time of the gas molecules becomes shorter, hence, little time is available to adsorb on the surface in the reaction chamber and therefore, demonstrate little degradation efficiency. It can be inferred from these results that a higher photodegradation efficiency can be achieved by optimizing the flow rate of the VOCs in the degradation system. For the comparison, the photodegradation experiment was also performed in the blank chamber (no catalysts) under similar conditions in order to exclude the oxidation effect of oxygen in the chamber under 400 W xenon lamp (Fig. 10). It is clear that no photodegradation occurs in the absence of TiO_2 catalyst. Additionally, the study confirms that the molecular structure of the gas molecule is an important parameter to be considered in order to design the potential photocatalyst.

4 Conclusion

In summary, the adsorption behavior of acetaldehyde and ethylene on TiO_2 {001} facets was successfully evaluated. TiO_2 NPs with dominant {001} facet were synthesized in strong acidic conditions by hydrothermal reaction. Acetaldehyde molecules demonstrated strong interaction with TiO_2 surface due to its carbonyl group molecular structure. In contrast to acetaldehyde, the ethylene has poor adsorption capacity and lower degradation rate. The results were further confirmed with the first principle calculations. The acetaldehyde molecule exhibited high adsorption energy, which might be associated with the formation of chemical bonds with (001) surface of TiO_2. However, ethylene demonstrated lower adsorption energy and no significant distortion on the surface could be traced, indicating the weak interaction of ethylene molecules with titania surface. This work is significant to understand the interaction of different VOCs with catalyst surface, which can be used for future references and designing potential catalysts for the remediation of pollutants from the environment.

Acknowledgement The authors are thankful for the financial support under the National Key Research and Development Program of China (2016YFA0203000), CAS President's International Fellowship Initiative (PIFI) program, NSFC-DFG bilateral organization program (51761135107).

Complaince with Ethical Standards

Conflict of interest The authors declared that they have no conflicts of interest to this work. We declare that we do not have any commercial or associative interest that represents a conflict of interest in connection with the work submitted.

References

1. Wu M, Leung DYC, Zhang Y et al (2019) Toluene degradation over Mn–TiO_2/CeO_2 composite catalyst under vacuum ultraviolet (VUV) irradiation. Chem Eng Sci 195:985–994
2. Stucchi M, Galli F, Bianchi CL et al (2018) Simultaneous photodegradation of VOC mixture by TiO_2 powders. Chemosphere 193:198–206
3. Li X, Li J, Shi Y et al (2018) Rational design of cobalt and nitrogen co-doped carbon hollow frameworks for efficient photocatalytic degradation of gaseous toluene. J Colloid Interface Sci 528:45–52
4. Jafari AJ, Kalantary RR, Esrafili A et al (2018) Synthesis of silica-functionalized graphene oxide/ZnO coated on fiberglass and its application in photocatalytic removal of gaseous benzene. Process Saf Environ Prot 116:377–387
5. Zhou H, Wen Z, Liu J et al (2019) Z-scheme plasmonic Ag decorated WO_3/Bi_2WO_6 hybrids for enhanced photocatalytic abatement of chlorinated-VOCs under solar light irradiation. Appl Catal B 242:76–84
6. Saqer SM, Kondarides DI, Verykios XE (2011) Catalytic oxidation of toluene over binary mixtures of copper, manganese and cerium oxides supported on γ-Al_2O_3. Appl Catal B 103(3):275–286
7. Tode R, Ebrahimi A, Fukumoto S et al (2010) Photocatalytic decomposition of water on double-layered visible light-responsive TiO_2 thin films prepared by a magnetron sputtering deposition method. Catal Lett 135(1):10–15
8. Hogan T, Simpson R, Lin M et al (1996) A broad spectrum catalytic system for removal of toxic organics from water by deep oxidation using dioxygen as the oxidant. Catal Lett 40(1):95–99

9. Pratap Reddy M, Phil HH, Subrahmanyam M (2008) Photocatalytic disinfection of *Escherichia coli* over titanium (IV) oxide supported on Hβ zeolite. Catal Lett 123(1):56
10. Ferentz M, Landau MV, Herskowitz M (2018) Relationship of crystals shape, aggregation mode and surface purity in catalytic wet peroxide oxidation of phenol in dark with titania anatase nanocrystals. Catal Lett 148(11):3524–3533
11. Pazhamalai P, Krishnamoorthy K, Mariappan VK et al (2019) Blue TiO_2 nanosheets as a high-performance electrode material for supercapacitors. J Colloid Interface Sci 536:62–70
12. Saltveit ME (1999) Effect of ethylene on quality of fresh fruits and vegetables. Postharvest Biol Technol 15(3):279–292
13. Adel AK (2003) A Perspective on postharvest horticulture (1978–2003). HortScience 38(5):1004–1008
14. Sawada S, Totsuka T (1967) Natural and anthropogenic sources and fate of atmospheric ethylene. Atmos Environ 20(5):821–832
15. Fu X, Clark LA, Yang Q et al (1996) Enhanced photocatalytic performance of titania-based binary metal oxides: TiO_2/SiO_2 and TiO_2/ZrO_2. Environ Sci Technol 30(2):647–653
16. Fu X, Clark LA, Zeltner WA et al (1996) Effects of reaction temperature and water vapor content on the heterogeneous photocatalytic oxidation of ethylene. J Photochem Photobiol A 97(3):181–186
17. Obee TN, Hay SO (1997) Effects of moisture and temperature on the photooxidation of ethylene on titania. Environ Sci Technol 31(7):2034–2038
18. Yamazaki S, Tanaka S, Tsukamoto H (1999) Kinetic studies of oxidation of ethylene over a TiO_2 photocatalyst. J Photochem Photobiol A 121(1):55–61
19. Park D-R, Zhang J, Ikeue K et al (1999) Photocatalytic oxidation of ethylene to CO_2 and H_2O on ultrafine powdered TiO_2 photocatalysts in the presence of O_2 and H_2O. J Catal 185(1):114–119
20. Ghosh D, Smith AR, Walker AB et al (2018) Mixed A-cation perovskites for solar cells: atomic-scale insights into structural distortion, hydrogen bonding, and electronic properties. Chem Mater 30(15):5194–5204
21. Bianchi CL, Gatto S, Pirola C et al (2014) Photocatalytic degradation of acetone, acetaldehyde and toluene in gas-phase: comparison between nano and micro-sized TiO_2. Appl Catal B 146:123–130
22. Huang H, Leung DYC, Ye D (2011) Effect of reduction treatment on structural properties of TiO_2 supported Pt nanoparticles and their catalytic activity for formaldehyde oxidation. J Mater Chem 21(26):9647–9652
23. Lin W, Xie X, Wang X et al (2018) Efficient adsorption and sustainable degradation of gaseous acetaldehyde and o-xylene using rGO-TiO_2 photocatalyst. Chem Eng J 349:708–718
24. Pan J, Liu G, Lu GQ et al (2011) On the true photoreactivity order of {001}, {010}, and {101} facets of anatase TiO_2 crystals. Angew Chem 123(9):2181–2185
25. Ren L, Li Y, Hou J et al (2016) The pivotal effect of the interaction between reactant and anatase TiO_2 nanosheets with exposed 001 facets on photocatalysis for the photocatalytic purification of VOCs. Appl Catal B 181:625–634
26. Kresse G, Furthmüller J (1996) Efficiency of ab initio total energy calculations for metals and semiconductors using a plane-wave basis set. Comput Mater Sci 6(1):15–50
27. Kresse G, Furthmüller J (1996) Efficient iterative schemes for ab initio total-energy calculations using a plane-wave basis set. Phys Rev B 54(16):11169–11186
28. Kresse G, Hafner J (1993) Ab initio molecular dynamics for liquid metals. Phys Rev B 47(1):558–561
29. Perdew JP, Burke K, Ernzerhof M (1996) Generalized gradient approximation made simple. Phys Rev Lett 77(18):3865–3868
30. Perdew JP, Chevary JA, Vosko SH et al (1992) Atoms, molecules, solids, and surfaces: applications of the generalized gradient approximation for exchange and correlation. Phys Rev B 46(11):6671–6687
31. Grimme S (2006) Semiempirical GGA-type density functional constructed with a long-range dispersion correction. J comput chem 27(15):1787–1799
32. Wang W, Lu C, Ni Y et al (2013) Crystal facet growth behavior and thermal stability of 001 faceted anatase TiO_2: mechanistic role of gaseous HF and visible-light photocatalytic activity. CrystEngComm 15(13):2537–2543
33. Peng C, Yang X, Li Y et al (2016) Hybrids of two-dimensional Ti_3C_2 and TiO_2 exposing 001 facets toward enhanced photocatalytic activity. ACS Appl Mater Interfaces 8(9):6051–6060
34. Jian-Feng WAN, D-SH HU, Peng-Hui LU, Bi-Zhou LIN, Yi-Lin CHEN, Bi-Fen GAO (2016) Preparation of anatase TiO_2 nanocube with exposed (001) facet and its photocatalytic properties. J Inorg Mater 31(8):845–849
35. Mao Y, Wong SS (2006) Size- and shape-dependent transformation of nanosized titanate into analogous anatase titania nanostructures. J Am Chem Soc 128(25):8217–8226
36. Araújo ES, Libardi J, Faia PM et al (2015) Hybrid ZnO/TiO_2 loaded in electrospun polymeric fibers as photocatalyst. J Chem 2015:10
37. Fonoberov VA, Balandin AA (2004) Interface and confined optical phonons in wurtzite nanocrystals. Phys Rev B 70(23):233205
38. Chandra M, Bhunia K, Pradhan D (2018) Controlled synthesis of CuS/TiO_2 heterostructured nanocomposites for enhanced photocatalytic hydrogen generation through water splitting. Inorg Chem 57(8):4524–4533
39. Pan J, Liu G, Lu GQ et al (2011) On the true photoreactivity order of 001}, {010}, and {101 facets of anatase TiO_2 crystals. Angew Chem Int Ed 123(9):2181–2185
40. Sun J, Wang Q, Wang W et al (2018) Study on the synergism of steam reforming and photocatalysis for the degradation of Toluene as a tar model compound under microwave-metal discharges. Energy 155:815–823
41. Liqiang J, Xiaojun S, Jing S et al (2003) Review of surface photovoltage spectra of nano-sized semiconductor and its applications in heterogeneous photocatalysis. Sol Energy Sol Cells 79(2):133–151
42. Xing M-Y, Yang B-X, Yu H et al (2013) Enhanced photocatalysis by Au nanoparticle loading on TiO_2 single-crystal (001) and (110) facets. J Phys Chem Lett 4(22):3910–3917
43. Araujo-Lopez E, Varilla LA, Seriani N et al (2016) TiO_2 anatase's bulk and (001) surface, structural and electronic properties: a DFT study on the importance of Hubbard and van der Waals contributions. Surf Sci 653:187–196

Affiliations

Gansheng Shi[1] · Asad Mahmood[1] · Guanhong Lu[1] · Xiao Wang[1] · Shengrui Tong[2] · Maofa Ge[2] · Xiaofeng Xie[1] · Jing Sun[1]

[1] The State Key Lab of High Performance Ceramics and Superfine Microstructure, Shanghai Institute of Ceramics, Chinese Academy of Sciences, 1295 Dingxi Road, Shanghai 200050, China

[2] Institute of Chemistry, Chinese Academy of Sciences, Beijing 100190, China